Lasers in Manufacturing Conference 2023

Optimization of the melt flow by adjusting the keyhole geometry with dynamic beam shaping during laser welding

Jonas Wagner[a*], Michael Haas[a,b], Felix Zaiß[a], Christian Hagenlocher[a], Rudolf Weber[a], Thomas Graf[a]

[a]*Institut für Strahlwerkzeuge (IFSW), Pfaffenwaldring 43, 70569 Stuttgart, Germany*
[b]*Graduate School of Excellence advanced Manufacturing Engineering, University of Stuttgart, Nobelstr. 12, 70569 Stuttgart, Germany*

Abstract

The melt flow determines major characteristics in laser welding such as temperature distribution and defects like humping and undercuts. The characteristics of the melt flow are mainly determined by its interaction with the keyhole wall. In order to optimize the melt flow, it is required to adjust the keyhole geometry. Recent fiber laser sources provide coherent beam combining in the range of several kilowatts optical power, which enables beam shaping with almost arbitrary variations of quasi-stationary intensity distributions. The influence of the beam shape on the keyhole geometry was experimentally captured by online highspeed records during welding of aluminum and steel. Subsequently the influence of the shapes on the characteristics of the fluid flow was experimentally and numerically analyzed. The obtained results prove the potential of coherent beam combining to optimize welding processes by means of arbitrary and independent adjustment of the fluid flow.

Keywords: beam shaping; laser welding; numerical analysis; melt flow; optimization

1. Introduction

The melt flow is an important feature in laser welding processes. It influences the temperature distribution, as shown by Rai et al., 2007, and has a direct relation to the formation of defects such as undercuts, as shown by Frostevarg and Kaplan, 2014 and humping, as presented by Berger et al., 2011. The characteristics of the melt flow are mainly determined by its interaction with the keyhole wall, as shown by Fabbro et al., 2007.

* Corresponding author. Tel.: +49(0) 711 685-66849; fax: +49(0) 711 685-66842.
E-mail address: Jonas.wagner@ifsw.uni-stuttgart.de.

Consequently, influencing the melt flow through shaping of the keyhole geometry is a suitable approach for process optimization. Examples for influencing the geometry of the keyhole are the application of multiple laser beams, as demonstrated by Reinheimer et al., 2022, the deflection of the laser beam with high frequencies by scanner optics, for example demonstrated by Jarwitz et al., 2018b and Fetzer et al., 2018 or the use of multi core fibers, as shown by Jarwitz et al., 2018a, Hollatz et al., 2023 - 2023, Punzel et al., 2020 and Wang et al., 2020.

Recent fiber laser sources, as presented by Shekel et al., 2020 provide coherent beam combining in the range of several kilowatts optical power, which enables beam shaping with almost arbitrary variations of quasi-stationary intensity distributions, and in particular the generation of non-rotationally symmetrical beam shapes. The application of this novel technology in laser welding and the ability to influence the keyhole geometry was recently demonstrated by Wagner et al., 2022. The new technology opens up novel possibilities and approaches for the improvement of laser material processing. Concomitantly, the high number of degrees of freedom poses new and complex challenges in determining the optimal parameters for the respective process.

In the present paper, we confirm from experimental results that in laser welding the geometry of the keyhole can be influenced by beam shaping. Based on this we propose the combination of a numerical model for the calculation of the fluid flow with Bayesian optimization for the determination of optimal keyhole geometries. This is demonstrated by the optimization of the thermal efficiency.

2. Influence of beam shaping on the keyhole geometry

In order to investigate the influence of beam shaping on the keyhole geometry three different beam shapes were generated with the OPA6 laser from Civan. With this laser the generation of almost arbitrary quasi static beam shapes is possible by alternating between discrete, different intensity distributions with switch times of less than 100 ns. Fig. 1 depicts the calculated average intensity distribution of the applied beam shapes. The beam shape in Fig. 1a consists of one constant intensity distribution, the beam shapes in Fig. 1b and Fig. 1c each consist of six discrete intensity distributions. The shape repetition frequency for iterating once over all six intensity distributions was set to the maximum of 1.67 MHz. The depicted images of the beam shapes correspond to an area of 1350 µm² on the surface of the work piece, resulting from the setup with a focusing lens with a focal length f_{lens} = 1500 mm and positioning the waist of the individual laser beam on the sample's surface.

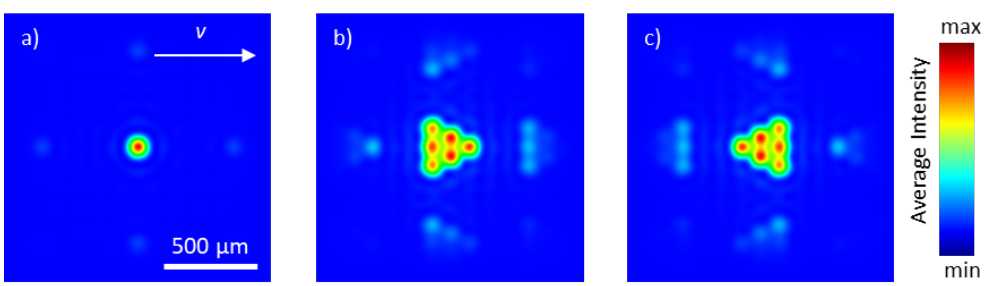

Fig. 1. Calculated average intensity distributions of the applied beam shapes with the OPA6 laser from Civan.

Samples of stainless steel 1.4301 were moved with a welding speed of v = 6 m/min below the static laser beam with a laser power of P_L = 4.5 kW. The orientation of the welding direction relative to the beam shapes is given by the white arrow in Fig. 1a. The process was recorded with a high-speed camera with a recording frequency of 10 kHz at an angle of ≈ 10° relative to the beam axis, transverse to the welding direction.

Fig. 2 shows images averaged over 8000 frames of the highspeed videos of the welding process with the different beam shapes. The welding direction was from left to right, as indicated by the white arrow in the top left. The position of the keyhole is highlighted by the orange arrows. For comparison the images in the bottom row (Fig. 2 d-f) show the images from the top row, augmented by an overlay of the corresponding beam shape.

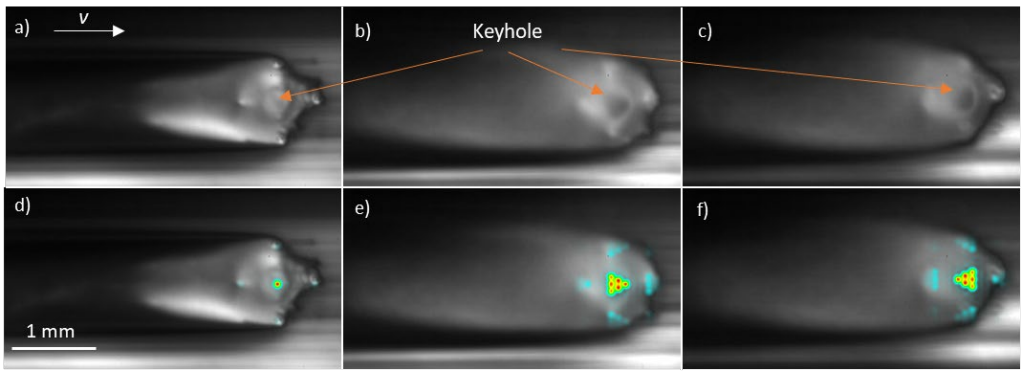

Fig. 2. Averaged highspeed images during welding of stainless steel with different beam shapes. Lower row: with overlays of the applied beam shapes. v = 6 m/min, 1.4301, P_L = 4.5 kW.

The images prove a significant influence of the applied beam shape on the opening of the keyhole. Furthermore, an influence of the side lobes next to the keyhole, in the melt pool is shown.

3. Model

The melt flow was optimized using a combination of a numerical model for the calculation of the melt flow and Bayesian optimization.

With this model two base cases were investigated, each with a triangular shape with axial symmetry along the weld's centerline. One with the tip pointing towards the welding direction, similar to the orientation in Fig. 2b and e and one with the tip pointing opposite to the welding direction, similar to the orientation in Fig. 2c and f. For the present paper the opening angle was optimized with the goal of a maximum thermal efficiency. The angle was adjusted by varying the width of the triangle. The length of the triangle in welding direction was constant at all trials with 750 µm. The range of possible opening angles during the optimization trials was defined as $0° \leq \alpha \leq 60°$.

3.1. Calculation of the melt flow

The melt flow was calculated with a CFD model as previously described by Wagner et al., 2021 in OpenFOAM, see Weller et al., 1998. With this model the melt flow around a static keyhole shape is determined under consideration of the phase change and the latent heat. The cylindrical keyhole in the model was replaced by the triangular shapes. As a heat source the temperature at the keyhole front was set equal to the material's evaporation temperature. The outcome of the model are the local temperature, phase, pressure and vectors of the local velocities in the melt and the surrounding material, after a simulated process time of 0.2 s.

3.2. Bayesian optimization

For the optimization the Ax platform was used, as described on Meta Platforms, Inc., 2023. Ax is based on the BoTorch framework for Bayesian optimization in PyTorch, which is described by Balandat et al., 2020. The application of Bayesian optimization in laser material processing is described in detail by Michalowski et al., 2023. With the applied model at first five initial experiments i.e., simulations are conducted with opening angles generated by a SOBOL sequence, as described by Sobol', 1967. In the subsequent optimization phase, 20 further experiments are carried out, in which the opening angle for the current trial is based on the outcome of all previous experiments and selected on the basis of the maximum expected improvement.

4. Optimization of the thermal efficiency

4.1. Model parameters

The described model can be used to optimize various features of the welding process. For the present paper this is demonstrated by means of the optimization of the thermal efficiency during laser welding of the aluminum alloy AA6016, which is specified in the norm DIN EN 573-3:2022-09. The material properties were chosen as given in the description of the model by Wagner et al., 2021, as specified by Kammer, 1998 and Leitner et al., 2017.

The red line in Fig. 3 presents exemplarily a temperature profile along a line transverse to the welding direction, at the position of the maximum melt pool width, during full penetration laser welding of aluminum. The position of the cross-section is indicated by the dash-dotted purple line in the sketch of the melt pool at the top right in Fig. 3.The blue hatched area marks the width where at least the melting temperature T_{melt} was reached. After solidification this yields the width of the cross-section of the weld seam. The required power

$$P_{req} = v \cdot w_{weld} \cdot s \cdot \rho \cdot \left(c_p \cdot \left(T_{liq} - T_0\right) + h_s\right) \quad (1)$$

results from the welding speed v, the width of the weld w_{weld}, the sheet's thickness s, the material properties density ρ, heat capacity c_p, liquidus temperature T_{liq}, latent heat of fusion h_s and the temperature before the beginning of the process T_0.

As shown in Fig. 3 the welding process also results in heating of the surrounding material, which is considered as heat losses. The thermal efficiency

$$\eta_{th} = \frac{P_{req}}{P_{abs}} \quad (2)$$

describes the ratio of the required laser power P_{req} to the totally absorbed laser power P_{abs} and is therefore a measure of how efficiently the available power is used. In order to increase this efficiency, the temperature distribution must be adjusted. The temperature distribution for a given heat input results from heat conduction, which is given by the material properties and from convection, which results from the characteristics of the melt flow. Influencing the melt flow therefore offers the potential to increase the thermal efficiency.

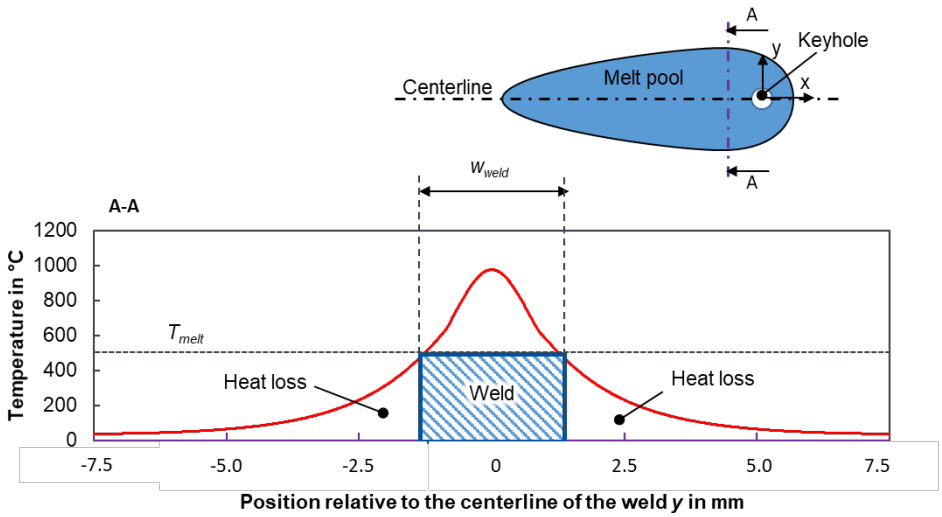

Fig. 3. Example of the temperature distribution during laser welding. Transverse to the welding direction, trough the position of the maximum width of the melt pool, as indicated with the purple dash-dotted line in the sketch at the top right.

4.2. Optimization

The charts in Fig. 4 show the thermal efficiency η_{th} for each trial during the progress of the optimization. Orange data points indicate results during welding with the tip of the triangle at the front, blue data points indicate results with an opposite orientation of the triangle with a flat frontside. The datapoints in Fig. 4a on the left show the thermal efficiency resulting from each trial, the datapoints in Fig. 4b on the right show the current optimal thermal efficiency after the corresponding number of trials. The blue semi-transparent area highlights the first five experiments, generated by the SOBOL sequence, without optimization.

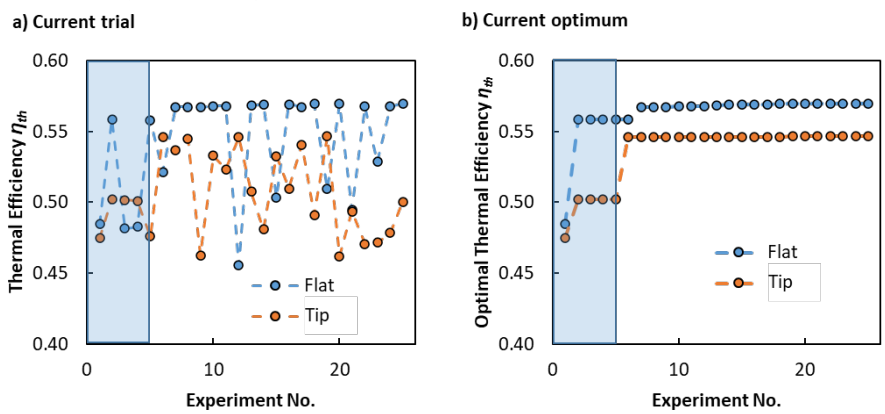

Fig. 4. Progress of the optimization of the opening angle of a triangular keyhole for increased thermal efficiency. Flat: Flat side of the keyhole in front, similar to Fig. 1c. Tip: Tip of the keyhole in front similar to Fig. 1b.

The data show that for both orientations suitable parameters for an increase of the thermal efficiency are determined through the optimization algorithm. In case of welding with a flat front the thermal efficiency is

increased from an initial maximum of 0.55, resulting from the random SOBOL sequence to 0.57 and in case of welding with the tip towards the front from 0.50 to 0.55.

Fig. 5 shows the thermal efficiency for both orientations of the triangles as a function of the opening angle α. The thermal efficiency is higher in case of welding with a flat front for all angles $\alpha > 25°$. In case of welding with the tip towards the front the thermal efficiency increases nearly linearly between 20° and 60°. For welding with a flat front, the increase is only linear between approximately 20° and 45°. With a further increase of the angle the thermal efficiency increases disproportionally stronger and plateaus at 0.57 for $\alpha > 55°$. The distinct range of optimum angles also results in an increased number of trials in this range during the optimization.

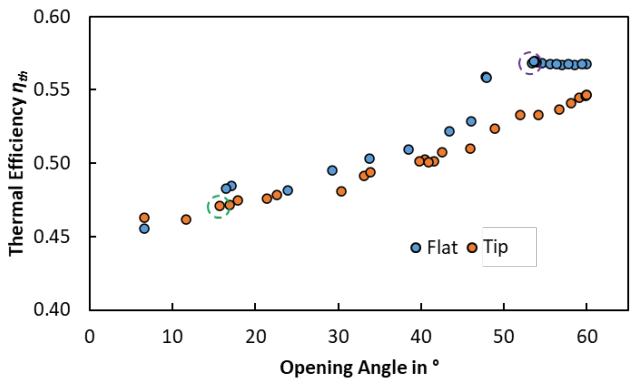

Fig. 5. Thermal efficiency as a function of the opening angle of a triangular keyhole. Flat: Flat side of the keyhole in front, similar to Fig. 1c. Tip: Tip of the keyhole in front similar to Fig. 1b. Full penetration welding of AA6016, calculated with the model from Wagner et al., 2021.

Fig. 6 compares the characteristics of the melt flow for two different keyhole geometries. Fig. 6a shows the melt flow during welding with the tip at the front and an opening angle of $\alpha = 12°$, resulting in $\eta_{th} = 0.46$, corresponding to the data point which is highlighted by the green dashed circle in Fig. 5. Fig. 6b shows the melt flow during welding with a flat front with $\alpha = 53°$, resulting in $\eta_{th} = 0.57$, corresponding to the data point which is highlighted by the purple dashed circle in Fig. 5. The colours indicate the local velocity of the melt, relative to the keyhole, according to the colour scale. The white arrows represent sections of streamlines. The black line outlines the melt pool boundary and the white triangular areas depict the keyhole areas. The welding direction is from left to right.

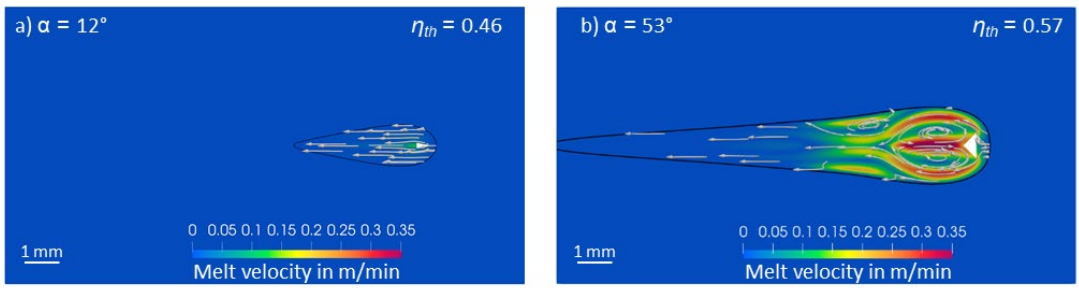

Fig. 6. Melt flow during full penetration laser welding of AA6016 with a triangular keyhole with different opening angles and orientations. Left: tip of the keyhole at the front, α = 12°, right: flat side of the keyhole at the front, α = 53°. Calculated with the model from Wagner et al., 2021.

In both examples the flow exhibits symmetry along the centreline of the weld. In case of welding with the tip at the front and the smaller opening angle $\alpha = 12°$, the melt flow is mostly parallel to the welding direction with minor deviations in the region of the keyhole. The melt velocities relative to the keyhole are low with a maximum of 0.12 m/min behind the keyhole.

In case of welding with the flat side at the front with the larger opening angle $\alpha = 53°$, two eddies form behind the keyhole with increased local melt velocities opposite to the welding direction at the side of the melt pool and towards the backside of the keyhole, with a maximum of 0.35 m/min.

5. Conclusion

The results show that the combination of CFD-models with Bayesian optimization is a suitable method for the use of modern beam shaping technologies, which provides for an unprecedented number of new parameter variants. In the present paper the opening angle of a triangular keyhole was chosen as the input parameter and the thermal efficiency as the optimization goal. A comprehensive analysis of the process efficiency, requires the consideration of the enthalpy of evaporation as well as the absorptance, which both also depend on the keyhole geometry. With the described model the optimization can be easily adapted for other and more input parameters and other output parameters which are available from the CFD-model. Furthermore, an optimization of multiple weighted goals is possible. This offers the potential for the development of tailored beam shaping strategies for specific welding applications.

Additionally, the results show that the new beam shaping methods make shaping of the melt flow a novel and promising strategy for process optimization.

Acknowledgements

This work was supported by Civan Advanced Technologies and Robert Bosch.

References

Balandat M., Karrer B., Jiang D. R., Daulton S., Letham B., Wilson A. G., Bakshy E., 2020. BoTorch: A Framework for Efficient Monte-Carlo Bayesian Optimization. In: Advances in Neural Information Processing Systems 33

Berger P., Hügel H., Hess A., Weber R., Graf T., 2011. Understanding of Humping Based on Conservation of Volume Flow. Physics Procedia 12, pp 232–240. doi: 10.1016/j.phpro.2011.03.030

DIN EN 573-3:2022-09, Aluminium und Aluminiumlegierungen_- Chemische Zusammensetzung und Form von Halbzeug_- Teil_3: Chemische Zusammensetzung und Erzeugnisformen; Deutsche Fassung EN_573-3:2019+A1:2022, Berlin

Fabbro R., Slimani S., Coste F., Briand F., 2007. Analysis of the various melt pool hydrodynamic regimes observed during cw Nd-YAG deep penetration laser welding. In: Congress proceedings 2007. Laser Institute of America, Orlando, Fla, p 802

Fetzer F., Sommer M., Weber R., Weberpals J.-P., Graf T., 2018. Reduction of pores by means of laser beam oscillation during remote welding of AlMgSi. Optics and Lasers in Engineering 108, pp 68–77. doi: 10.1016/j.optlaseng.2018.04.012

Frostevarg J., Kaplan A. F., 2014. Undercuts in Laser Arc Hybrid Welding. Physics Procedia 56, pp 663–672. doi: 10.1016/j.phpro.2014.08.071

Hollatz S., Hummel M., Lach M.-C., Olowinsky A., Gillner A., Häfner C., Beckmann F., Moosmann J., 2023 - 2023. Influence of ring-shaped laser beam during welding of AW-5083 and AW-6082. In: Kleine KR, Kaierle S (eds) High-Power Laser Materials Processing: Applications, Diagnostics, and Systems XII. SPIE, p 24

Jarwitz M., Lind J., Weber R., Graf T., Speker N., Haug P., 2018a. Investigation of the influence of superimposed intensity distributions on the spatter behavior in laser welding of steel using online x-ray diagnostics. International Congress on Applications of Lasers & Electro-Optics 2018, p 703. doi: 10.2351/7.0004024

Jarwitz M., Fetzer F., Weber R., Graf T., 2018b. Weld Seam Geometry and Electrical Resistance of Laser-Welded, Aluminum-Copper Dissimilar Joints Produced with Spatial Beam Oscillation. Metals 8, p 510. doi: 10.3390/met8070510

Kammer C. (1998). Aluminium-Taschenbuch, 15th edn. Aluminium-Verlag, Düsseldorf

Leitner M., Leitner T., Schmon A., Aziz K., Pottlacher G., 2017. Thermophysical Properties of Liquid Aluminum. MTA 48, pp 3036–3045. doi: 10.1007/s11661-017-4053-6

Meta Platforms, Inc., 2023. Ax. Adaptive Experimentation Platform. https://ax.dev/. Accessed 9 June 2023

Michalowski A., Ilin A., Kroschel A., Karg S., Stritt P., Dais A., Becker S., Kunz G., Sonntag S., Lustfeld M., Tighineanu P., Onuseit V., Haas M., Graf T., Ridderbusch H., 2023 - 2023. Advanced laser processing and its optimization with machine learning. In: Gemini L, Narazaki A, Kleinert J (eds) Laser Applications in Microelectronic and Optoelectronic Manufacturing (LAMOM) XXVIII. SPIE, p 4

Punzel E., Hugger F., Dinkelbach T., Bürger A., 2020. Influence of power distribution on weld seam quality and geometry in laser beam welding of aluminum alloys. Procedia CIRP 94, pp 601–604. doi: 10.1016/j.procir.2020.09.086

Rai R., Elmer J. W., Palmer T. A., DebRoy T., 2007. Heat transfer and fluid flow during keyhole mode laser welding of tantalum, Ti–6Al–4V, 304L stainless steel and vanadium. J. Phys. D: Appl. Phys. 40, pp 5753–5766. doi: 10.1088/0022-3727/40/18/037

Reinheimer E. N., Weber R., Graf T., 2022. Influence of the capillary geometry on the weld seam quality during high-speed laser welding. Procedia CIRP 111, pp 431–434. doi: 10.1016/j.procir.2022.08.181

Shekel E., Vidne Y., Urbach B., 2020. 16kW single mode CW laser with dynamic beam for material processing. In: Dong L, Zervas MN (eds) Fiber Lasers XVII: Technology and Systems. SPIE, p 73

Sobol' I., 1967. On the distribution of points in a cube and the approximate evaluation of integrals. USSR Computational Mathematics and Mathematical Physics 7, pp 86–112. doi: 10.1016/0041-5553(67)90144-9

Wagner J., Berger P., He P., Fetzer F., Weber R., Graf T., 2021. Reduced finite-volume model for the fast numerical calculation of the fluid flow in the melt pool in laser beam welding. IOP Conf. Ser.: Mater. Sci. Eng. 1135, p 12010. doi: 10.1088/1757-899X/1135/1/012010

Wagner J., Heider A., Ramsayer R., Weber R., Faure F., Leis A., Armon N., Susid R., Tsiony O., Shekel E., Graf T., 2022. Influence of dynamic beam shaping on the geometry of the keyhole during laser beam welding. Procedia CIRP 111, pp 448–452. doi: 10.1016/j.procir.2022.08.185

Wang L., Mohammadpour M., Yang B., Gao X., Lavoie J.-P., Kleine K., Kong F., Kovacevic R., 2020. Monitoring of keyhole entrance and molten pool with quality analysis during adjustable ring mode laser welding. Appl Opt 59, pp 1576–1584. doi: 10.1364/AO.383232

Weller H. G., Tabor G., Jasak H., Fureby C., 1998. A tensorial approach to computational continuum mechanics using object-oriented techniques. Int. J. Numer. Meth. Engng 12, p 620. doi: 10.1063/1.168744